

Accepted Manuscript

Heterogeneous nucleation of pure Al on MgO single crystal substrate accompanied by a MgAl₂O₄ buffer layer

Jie Sun, Dingpu Wang, Yunhu Zhang, Cheng Sheng, Matthew Dargusch, Gui Wang, David St John, Qijie Zhai

PII: S0925-8388(18)31586-X

DOI: [10.1016/j.jallcom.2018.04.263](https://doi.org/10.1016/j.jallcom.2018.04.263)

Reference: JALCOM 45901

To appear in: *Journal of Alloys and Compounds*

Received Date: 20 January 2018

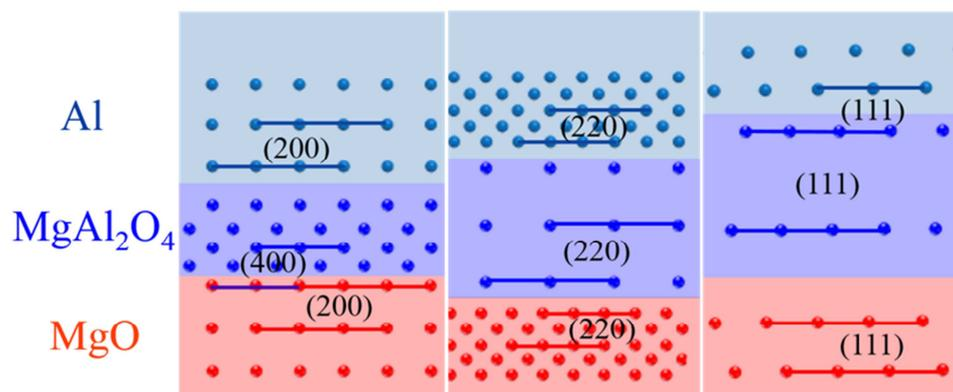
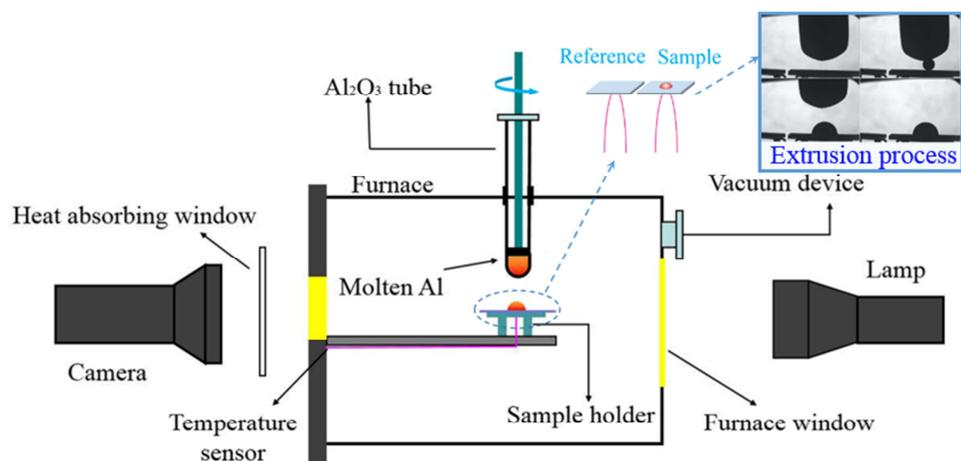
Revised Date: 20 April 2018

Accepted Date: 23 April 2018

Please cite this article as: J. Sun, D. Wang, Y. Zhang, C. Sheng, M. Dargusch, G. Wang, D. St John, Q. Zhai, Heterogeneous nucleation of pure Al on MgO single crystal substrate accompanied by a MgAl₂O₄ buffer layer, *Journal of Alloys and Compounds* (2018), doi: 10.1016/j.jallcom.2018.04.263.

This is a PDF file of an unedited manuscript that has been accepted for publication. As a service to our customers we are providing this early version of the manuscript. The manuscript will undergo copyediting, typesetting, and review of the resulting proof before it is published in its final form. Please note that during the production process errors may be discovered which could affect the content, and all legal disclaimers that apply to the journal pertain.





37 the study of heterogeneous nucleation has been an important topic in the metal
38 solidification field for decades, attracting numerous researchers using various
39 techniques and materials to meet industrial requirements and for alloy chemistry. In
40 general, the nucleating potency of a heterogeneous substrate can be attributed to
41 structure mismatch and orientation between solid to be nucleated and substrate,
42 material chemistry including interaction and segregation to the interface, and
43 temperature such as undercooling. Theoretically, a number of factors affecting the
44 nucleation potency include ~~the effect of the size and size~~ distribution of the nucleating
45 particles [3, 4], the surface roughness of a substrate [5], the cavity geometry of
46 substrates [6], the structure and composition of the nucleating surface [7], and the
47 chemical reaction between the liquid metal and substrates [8].

48

49 In a study on nucleation catalysis in supercooled liquid tin, Sundquist [9] postulated
50 that the nucleus is a layer of atoms adsorbed on the flat substrate when liquid tin
51 nucleates with a low undercooling, and the adsorbed layer can be arranged as a
52 nucleation embryo in the liquid. Oh et al. confirmed that an in-plane, ordered pure Al
53 atomic layer exists at the liquid Al/solid Al_2O_3 interface through experimental
54 investigation [10]. The latest experimental and theoretical studies all suggest that the
55 adsorbed layer formed at the liquid/substrate interface is a general phenomenon for a
56 nucleation interface and may impose important effects on nucleation [11]. The
57 adsorption layer can be described as a solid-like precursor, and the lattice
58 mismatching between the precursor and substrates then becomes the major energy
59 barrier for the nucleation of liquid. It means that the lattice misfit between substrates
60 and precursor becomes essential to determine if nucleation will occur [12-14]. Much
61 of the research involving $\text{Al}_3\text{Ti}/\text{TiB}_2$ suggests that the interface composition and
62 structure are the key points to improving the potency of nucleation [4, 15]. Recently,
63 Wang et al. [11] and Li et al. [16] studied the segregation of Cu at the interface
64 between the Al_2O_3 substrate and the Al-Cu alloy. The solute element, in this case Cu,
65 can modify the lattice matching of the nucleation interface, and the preferred crystal
66 orientation was affected by the substrate structure. Based on the lattice misfit effect on
67 heterogeneous nucleation, Wang et al. have carried out a series of experiments with
68 varied lattice misfits by changing the Al_2O_3 crystal plane of the substrate and
69 formulating the experimentally measured undercooling with corresponding lattice
70 misfits [17] and proposed an integrated model to predict the nucleation undercooling.
71 Experimental studies by Perepezko's team [18-20] and computer simulations [21]
72 have all indicated that the orientation relationship and lattice mismatch between
73 substrate and nucleus are important factors that influence the potency of the substrate
74 and the undercooling required for nucleation. The better the lattice matching is, the
75 higher the nucleation potency. Minimization of strain energy at the interfacial
76 boundaries between the two phases requires good atomic matching. Brown et al. [22]
77 observed in situ the orientation relationship of the interface plane between the
78 substrate and nucleus, and also revealed it would affect the potency of the substrate
79 and the required undercooling for nucleation.

80

81 MgO and MgAl₂O₄ are believed to be effective heterogeneous nucleating agents for
82 Al based alloys due to their similar lattice structures and small lattice misfits [23, 24].
83 However, most information on the interaction of molten aluminum with MgO was,
84 until now, gathered through wetting experiments, within temperature ranges up to
85 1137°C. Fujii et al. [25] identified the presence of Al₂O₃ at the interface between the
86 MgO and liquid Al. McEvoy et al. [26] reported that the reaction product of molten Al
87 with MgO was MgAl₂O₄. Morgile et al. [27] clarified that the MgAl₂O₄ was an
88 intermediate product and that Al₂O₃ was a final product of the reaction. It should be
89 noted here that most researchers [8, 23, 25-28] reported that interfacial reaction
90 between molten Al and MgO substrates occurred at a much higher temperature than
91 the normal casting temperature between 700-800°C. Zhang et al. [8] have investigated
92 the nucleation mechanism of Al nuclei on MgO at the experimental temperature of
93 1027°C, and found that the nucleation behavior is more complicated due to the varied
94 chemical reaction at this high temperature. Nevertheless, less attention has been paid
95 to the nucleation behavior of pure Al melt on MgO substrate and the generated
96 reaction products at the normal casting temperature. In addition, no literature has been
97 reported with respect to the formation of a perfect crystal and the orientation
98 relationship between the MgO crystal and reaction products.

99
100 In this work we utilized thermal analysis and high resolution transmission electron
101 microscopy to study the nucleation behavior of molten Al on single crystal MgO
102 substrates, using a differential scanning calorimeter (DSC) incorporating an image
103 capture system and a sessile drop system. The aim of this paper was to clarify the
104 reaction product and the corresponding orientation relationships at the interface of
105 Al/MgO heated to a maximum temperature of 750°C, and present the resulted
106 undercooling to understand the heterogeneous nucleation of molten Al on single
107 crystal MgO.

109 2. Experimental apparatus and procedure

110
111 As illustrated in Fig 1, a modified DSC measurement apparatus (Thermal Analysis
112 Company, Selb Germany) has been used to investigate heterogeneous nucleation, with
113 the apparatus consisting of four parts: furnace, image acquisition system, extrusion
114 device, and evacuating system with a rotary pump and a turbo molecular pump.

115
116 MgO and MgAl₂O₄ single crystals with dimensions of 14×10×0.5 mm³, used as
117 substrates in this study were purchased from Shanghai Hengda Optics and Fine
118 Mechanics Co., Ltd. These single crystals were polished to an average roughness (Ra)
119 of less than 1 nm using a nano-diamond slurry. Ultrahigh purity aluminum (99.9995%)
120 was employed as the solid to be nucleated in experimentation. Prior to the DSC
121 experiment, both the substrate and Al specimen were immersed in acetone and
122 ultrasonically cleaned, then the substrate was placed horizontally on the temperature
123 sensor while the Al specimen was placed in a high purity alumina tube with a 1 mm

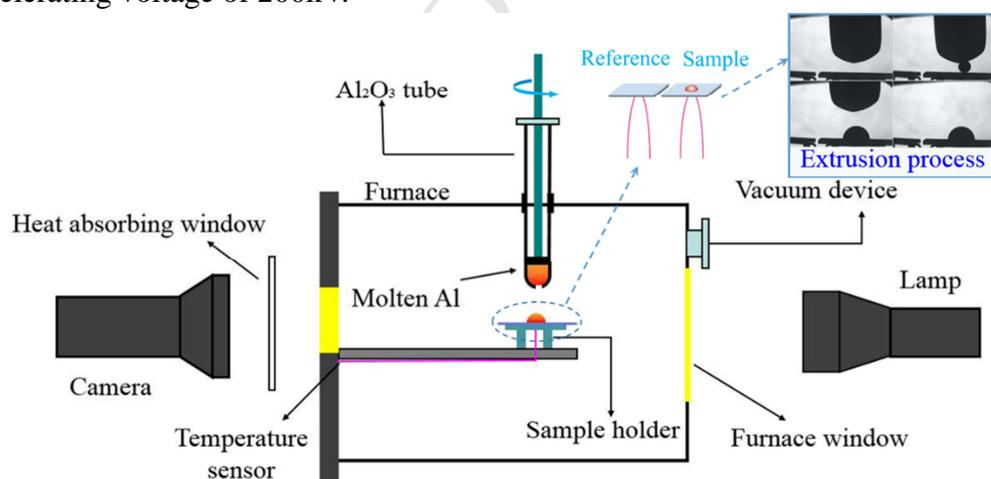
124 diameter hole in the bottom.

125

126 The furnace was first evacuated to 5×10^{-5} Pa, and then heated to the designed
 127 temperature of 750°C in a vacuum with a heating rate of $15^\circ\text{C}/\text{min}$. The alumina tube
 128 can be evacuated through the hole at the bottom keep the same atmosphere with the
 129 furnace. The chamber was filled with high purity argon with oxygen content less than
 130 0.1 ppm, and then molten Al was extruded through a hole at the bottom of the alumina
 131 tube and dropped onto a single crystal substrate to keep 3 mins at temperature of
 132 750°C before cooling. In this way, the initial oxide on the Al surface was
 133 mechanically removed as the liquid passed through the hole. In the current
 134 experimental set up, the hemispherical droplet sample was kept at about 1.5 mm in
 135 diameter. The sample was cooled at a rate of $15^\circ\text{C}/\text{min}$. After cooling down to room
 136 temperature, the Al sample with the substrate was removed from the chamber. The
 137 temperature was recorded by a platinum-rhodium-platinum thermocouple with an
 138 accuracy of $\pm 0.1^\circ\text{C}$. The experiments were repeated four times to ensure the
 139 repeatability of the experiments and the reliability of the results.

140

141 The crystal structure of solidified samples at the interface was characterized using
 142 high-resolution transmission electron microscopy (HRTEM) technique. Thin
 143 cross-sectional foil samples for HRTEM observation were prepared according to
 144 standard metallographic practice, and then milled by focused ion beam (FIB) using a
 145 FEI 600i dual-beam system under the condition of 30kV . Conventional TEM and
 146 HRTEM analyses were conducted using a JEM-2100F microscope operated at an
 147 accelerating voltage of 200kV .



148

149

Fig.1 Schematic illustration of the improved DSC measurement

150

3. Results

151

3.1 Nucleation undercooling

152

Fig. 2 presents measured DSC curves at the cooling rate of $15^\circ\text{C}/\text{min}$ for the liquid Al solidified on the different MgO substrates with (100), (110) and (111) crystal planes.

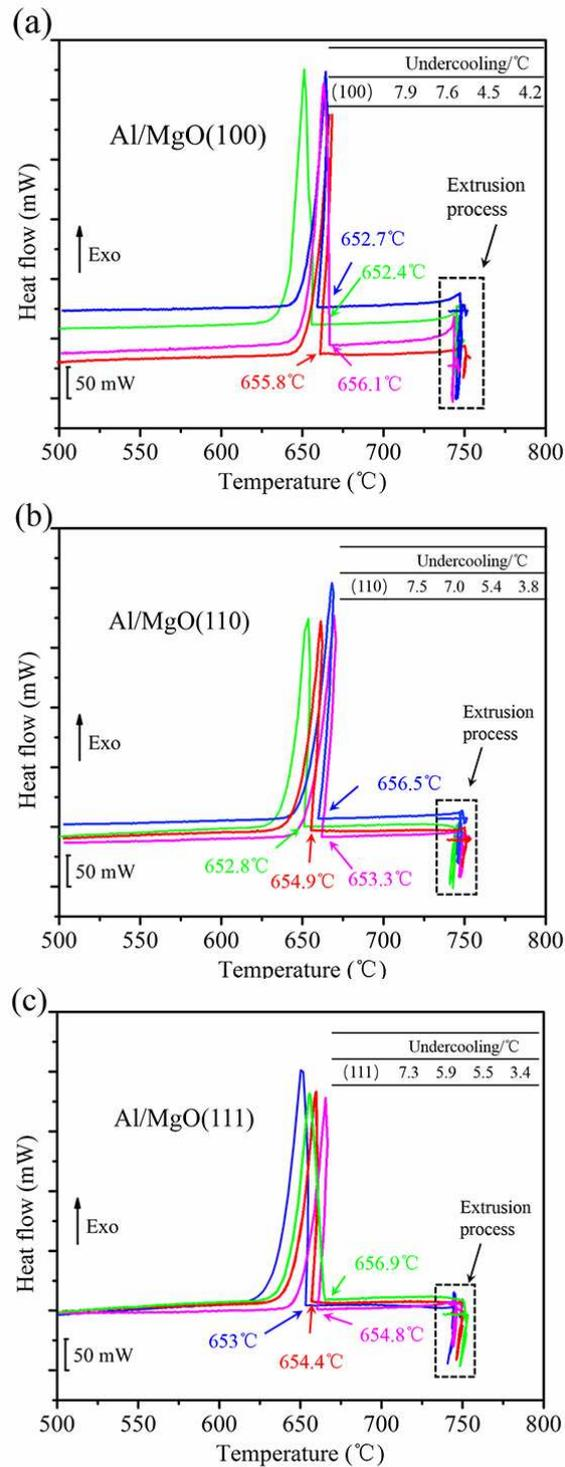
153

154

In this study, the undercooling is defined as the temperature difference between the equilibrium melting temperature (660.3°C) and the nominal start of solidification

155

156 temperature T_s . As shown in Fig. 2, the value of T_s achieved in the twelve DSC
157 experiments are varied between 652.7 and 656.9°C. In addition, the variation of T_s
158 can be observed even if the DSC measurements were repeatedly performed by using
159 the substrate with the same crystal plane. Fig.2 also shows the corresponding
160 undercooling ($\Delta T = 660.3 - T_s$) of Al on MgO substrates with the three different
161 crystal planes. The fluctuation of undercooling, varied from 3.4°C to 7.5°C, can be
162 found in these twelve DSC experiments of Al/MgO. Moreover, since the fluctuation
163 range is almost the same by comparing the achieved undercooling of Al solidified on
164 MgO substrates with different crystal planes, it indicates that the undercooling is not
165 influenced by the crystal planes of the MgO substrate.
166



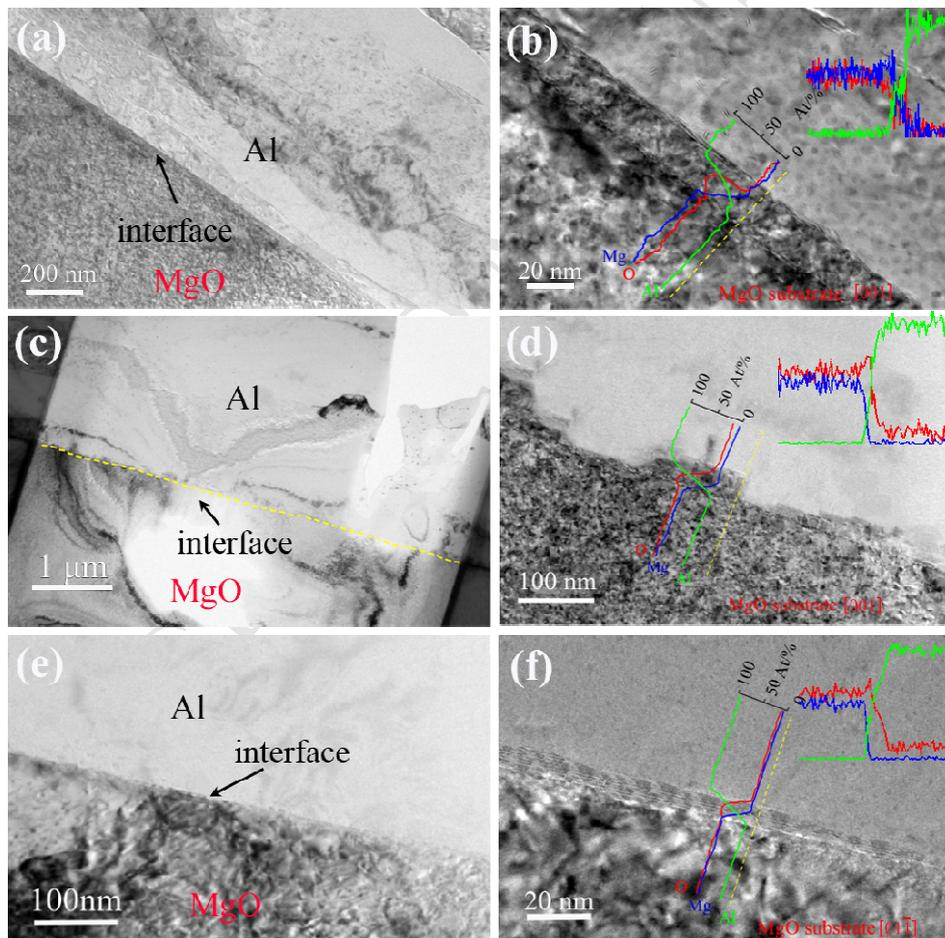
167

168 Fig.2 DSC solidification exotherms of Al droplet on MgO substrate with different
 169 lattice planes of (a) (100), (b) (110) and (c) (111) at the cooling rate of 15°C/min (The
 170 curves with 4 different colours means that the DSC experiments are repeated four
 171 times with different samples).

172

173 3.2 Characterization of Al/MgO interfaces

174 In order to further investigate the crystallographic orientation and variation of
 175 nucleation behavior, samples solidified on (100), (110) and (111) planes of MgO
 176 substrates were examined using TEM and HRTEM. Fig. 3 (a-f) shows the TEM
 177 images and EDS on the interfaces between the new crystal and MgO substrates. It can
 178 be observed that these interfaces are straight and distinct, and intermediate layers with
 179 distinct image contrast can be distinguished between the aluminum and MgO
 180 substrate. The thickness of the intermediate layer is between 10 and 40 nm. In
 181 addition, the intermediate layer in Fig. 3(b) and (f) is continuous and straight, which
 182 differs from the small islands and local formations in Fig. 3(d). With TEM-EDS
 183 analysis, it was confirmed that the upper right area corresponds to Al phase, while the
 184 lower left is the MgO substrate. The EDS mapping clearly shows that the distribution
 185 of the Mg, O and Al elements is similar in the intermediate layers of these three
 186 samples respectively solidified on MgO substrates of (100), (110) and (111) planes. It
 187 indicates that the generated intermediate layers, composed of aluminum, oxygen and
 188 magnesium, may be the same phase in these three samples. ~~Aside from this layer, the~~
 189 ~~Al and MgO substrates were also presented.~~



190

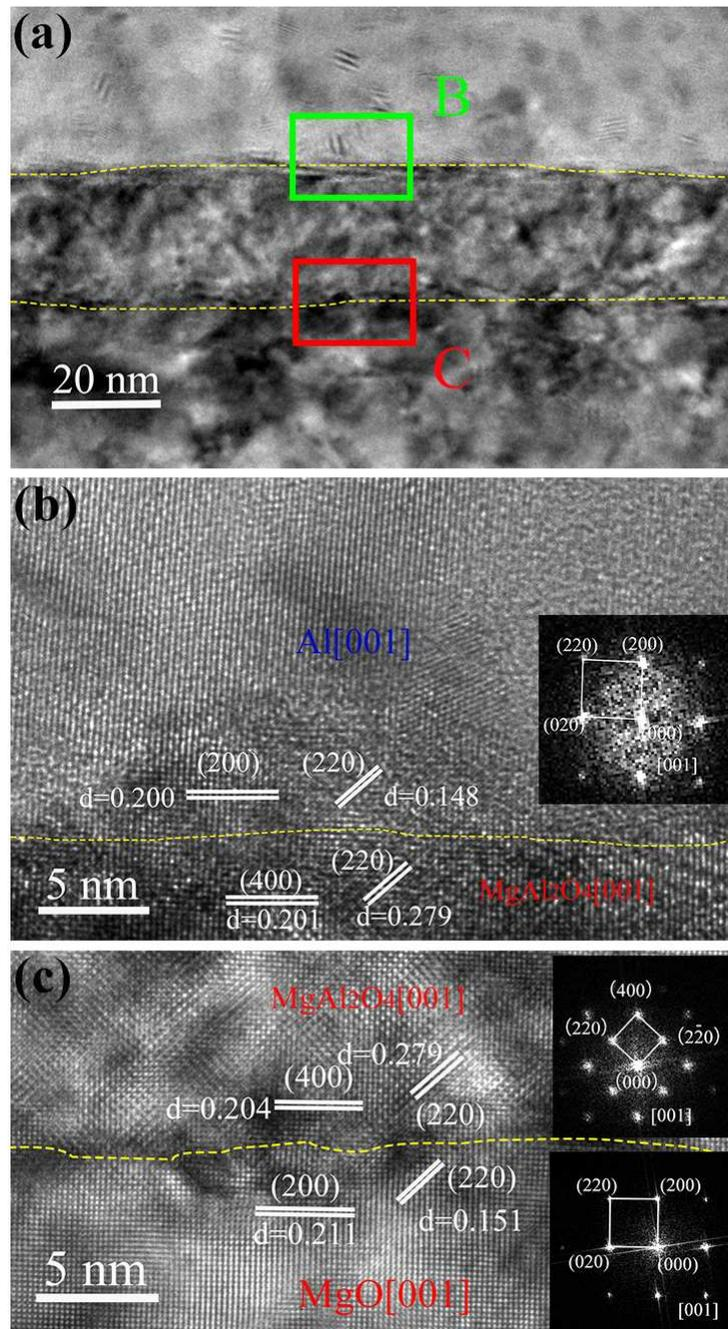
191 Fig.3 TEM images of (a) Al/(100)MgO, (c) (110)MgO, (e) (111)MgO nucleation
 192 interface take along MgO [001],[001] and $[01\bar{1}]$, separately. And corresponding EDS
 193 of (b),(d),(f), and the accompanying lines showing distribution of oxygen, magnesium
 194 and aluminum.

195 To further investigate the phase composition and structure of the nucleation surface,

196 samples solidified on (100), (110) and (111) planes were examined using HRTEM.

197

198 **Al/MgO (100) interface.** The HRTEM image of cross sections of the Al/MgO (100)
199 interface are shown in Fig. 4. The formed intermediate layer completely takes up the
200 interface of MgO, which means that it would act as a new nucleation substrate. Fig.
201 4(b) and (c) show a magnified HRTEM image of the interface viewed along the [001]
202 zone axis of the MgO substrate. Well-defined atomic rows and lattice planes can be
203 identified. Fast Fourier transformation (FFT) analysis indicates that the intermediate
204 layer is a face-centered cubic (FCC) structure with the spacing of 0.201-0.204 nm and
205 0.279 nm, which corresponds to the spacing of MgAl₂O₄ (400) and (220), respectively.
206 Since both the crystal structure and lattice spacing are consistent with that of
207 MgAl₂O₄ (FCC, $a=0.804$ nm) rather than α -Al₂O₃ with the hexagonal close packed
208 (HCP) structure and lattice spacing of $a=0.475$ nm and $c=1.297$ nm, it means that the
209 phase of the intermediate layer is only composed of MgAl₂O₄. Moreover, as shown in
210 Fig. 4(c), it can be found that the (400) plane of MgAl₂O₄ is perfectly parallel to the
211 (200) plane of the interface of the MgO substrate because the lattice arrangement of
212 (400) is identical to that of (200). The lattice arrangement of Al and the new phase
213 MgAl₂O₄ is clearly observed in Fig.4(b). Using FFT analysis, it was found that the
214 (200) planes of Al have a d -spacing of 0.200 nm and are parallel to the (400) planes of
215 the MgAl₂O₄ phase with a d -spacing of 0.201 nm. According to the presented lattice
216 plane shown in Fig. 4, the orientation relationship can be summed up as [001] (400)
217 MgAl₂O₄// [001] (200) MgO and [001] (220) MgAl₂O₄// [001] (220) Al.

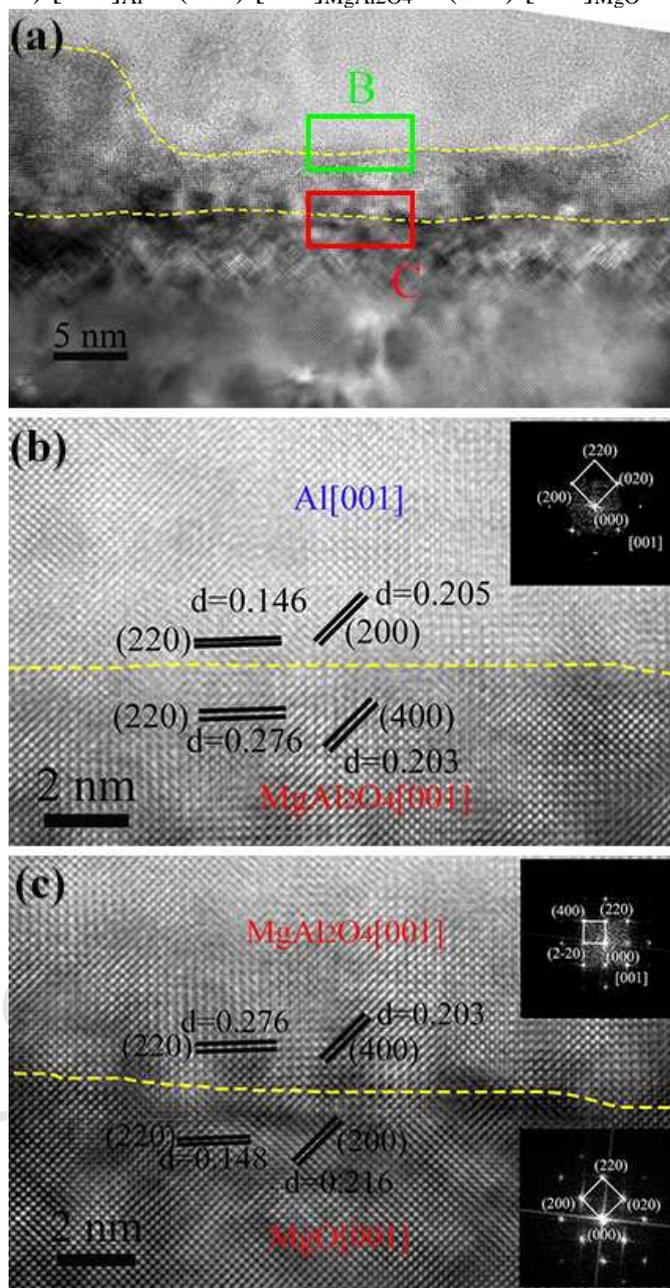


218
219
220
221
222

Fig.4 HRTEM image of Al/MgO(100) taken along [001] MgO zone direction (a); image of HRTEM of Al/MgAl₂O₄ interface, which corresponds to frame (B) of (a), and the FFT image of HRTEM (b); image of HRTEM of MgAl₂O₄/MgO interface, corresponding to frame (C) of (a), and the FFT image of HRTEM (c)

223 **Al/MgO (110) interface.** Fig. 5 is the HRTEM image of the sample solidified on the
224 MgO (110) plane, with the Al crystal being viewed along its [001] zone axis. The
225 interface of Al, intermediate layer and MgO were clearly seen in the Fig. 5(a),
226 respectively, which are marked with yellow dashed lines. Fig. 5(b) and (c) display a
227 magnifying HRTEM image of the interface, which was of selected area in Fig. 5(a).
228 Through FFT analysis of the HRTEM, the interplanar crystal spacing of the MgO
229 substrate was 0.148 nm and 0.216 nm, and they respectively correspond to the planes
230 of (220) and (200). It is worth noting that the lattice structure of MgO (220) is

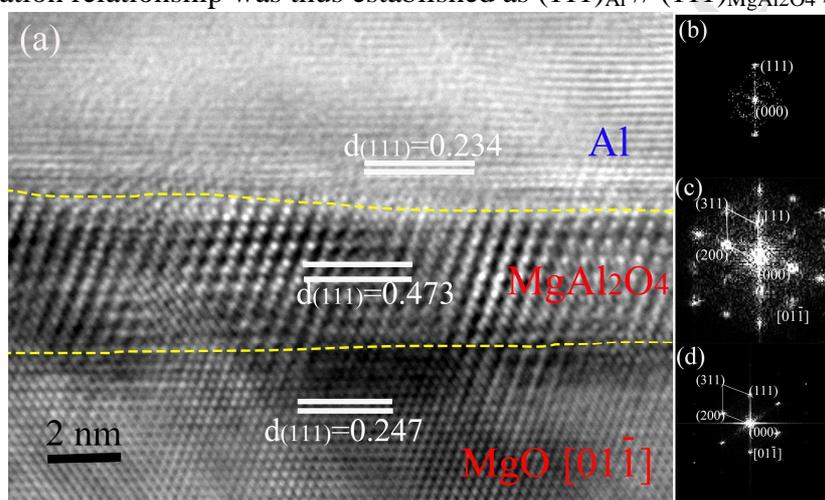
231 identical to that of (110), therefore, the (110) plane of MgO is parallel to the interface.
 232 Meanwhile, the intermediate layer is a FCC structure with d-spacing of 0.203 and
 233 0.276 nm respectively corresponding to the (400) and (220) planes, which suggests
 234 that the intermediate layer is also MgAl₂O₄. In addition, it was also noted that the
 235 (220) and (200) planes of MgO are perfectly parallel to the (220) and (400) planes of
 236 MgAl₂O₄, while being parallel to the (220) and (200) Al planes. In other words, the
 237 orientation relationship among them is (220) [001]_{Al} // (220) [001]_{MgAl₂O₄} // (220)
 238 [001]_{MgO}, and (200) [001]_{Al} // (400) [001]_{MgAl₂O₄} // (200) [001]_{MgO}.



239 Fig.5 HRTEM image of Al/MgO(110) take along [001] MgO zone direction and the
 240 FFT image of HRTEM(a); image of HRTEM of Al/MgAl₂O₄ interface, which
 241 corresponds to frame (B) of (a), and the FFT image of HRTEM (b); image of HRTEM
 242 of MgAl₂O₄/MgO interface, corresponding to frame (C) of (a), and the FFT image of
 243 HRTEM (c)
 244

245

246 **Al/MgO (111) interface.** A similar analysis method was adopted to observe the
 247 interface in Al/MgO (111) with the incident electron beam being parallel to the $[01\bar{1}]$
 248 axis of MgO, as shown in Fig. 6. The interface was marked with a yellow dashed line.
 249 The FFT image is shown in Fig. 6 by taking a Fourier transform of the HRTEM. The
 250 FFTs correspond to Al, MgAl_2O_4 and MgO, separately. The interplanar spacing in the
 251 middle area was consistent with a FCC structure with spacing of 0.473 nm for the
 252 (111) lattice plane. Since the crystal structure and the corresponding spacing shown in
 253 the middle area is also the same as that of MgAl_2O_4 , it means that the produced
 254 intermediate layer is still MgAl_2O_4 as already found in Al/MgO (100) and (110).
 255 Moreover, TEM examination confirmed that the reaction product MgAl_2O_4 displays
 256 the (111) plane as the natural surface. It can be seen that the (111) plane of MgAl_2O_4
 257 is parallel to the (111) plane of MgO and Al as well as the interface, as shown in Fig.6.
 258 The orientation relationship was thus established as $(111)_{\text{Al}} // (111)_{\text{MgAl}_2\text{O}_4} // (111)_{\text{MgO}}$.



259

260 Fig.6 HRTEM image of Al/MgO(111) take along $[01\bar{1}]$ MgO zone direction(a) and
 261 the FFT images of HRTEM(b),(c) and (d)
 262

262

263

4. Discussion

264

4.1 Formation of MgAl_2O_4 on the Al/MgO interfaces

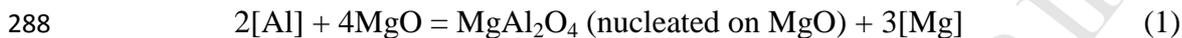
265

266 A number of researchers have investigated the interfacial reaction on the Al/MgO
 267 system [8, 23, 26-29]. Zhang et al [8] reported the reaction products of Al_2O_3 and
 268 MgAl_2O_4 between liquid Al and MgO at the temperature of 1027°C for 30 s, and
 269 similar reaction products formed on the interface were also found by Morgiel et al
 270 [27]. However, when investigating the wetting of molten Al on the MgO substrate in
 271 the temperature range of 1000°C to 1200°C , Shen et al [29] found that more complex
 272 interfacial reactions produced different phases of Al_2O_3 on Al/MgO systems, with no
 273 MgAl_2O_4 being detected. In their study, the final reaction products have been
 274 identified as primarily $\alpha\text{-Al}_2\text{O}_3$ phase for (100) MgO and κ' -, κ - and $\delta\text{-Al}_2\text{O}_3$ phases
 275 for (110) and (111) MgO, without a pronounced MgAl_2O_4 phase [29]. McEvoy et al
 276 [26] investigated the Mg concentration profile in a section of MgAl_2O_4 formed
 277 through interfacial reaction between molten Al and MgO. Their experimental results

278 revealed that the reactions between Al and MgO substrate are sensitive to the
 279 substrate orientation. Since the oxygen framework in MgO is quite similar to that in
 280 MgAl_2O_4 , the layer may be supposed to grow epitaxially by diffusion of Al or Mg
 281 metals through a relatively unchanged oxygen lattice[26]. However, our experimental
 282 results demonstrate that only the MgAl_2O_4 phase is produced as a new substrate to
 283 connect the Al and MgO regardless of the substrate orientation when the Al melt was
 284 cooled from 750°C.

285

286 After the molten aluminum was dropped on the substrates in the present study, the
 287 following chemical reaction[27, 30] may take place:



289 The brackets indicate that the elements were in liquid state. In reality, the reaction
 290 direction is dependent on the change of the Gibbs free energy for the reaction ΔG_r . If
 291 ΔG_r is negative, the direct reaction could take place. Otherwise, the reverse reaction
 292 would occur. According to Equation (1), the changes in the Gibbs free energy for the
 293 reaction can be described as:

$$\Delta G_r = \Delta G_f^o(\text{MgAl}_2\text{O}_4) - 4\Delta G_f^o(\text{MgO}) + RT \ln\left(\frac{\alpha_{\text{Mg}}^3}{\alpha_{\text{Al}}^2}\right) \quad (2)$$

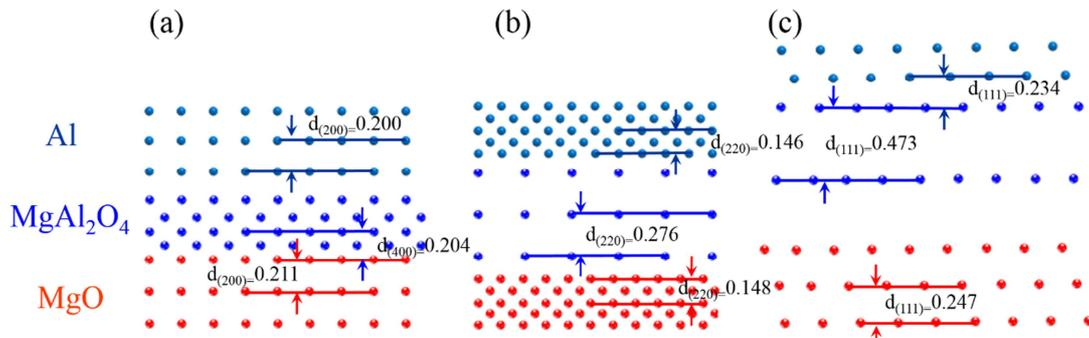
295 where $\Delta G_f^o(i)$ is the standard Gibbs free energy change of formation (J/mol), R is the
 296 gas constant (J/(mol·K)), T is the absolute temperature (K) and α_j is the activity of
 297 component j in the solution. The thermodynamic conditions of the reaction of MgO,
 298 MgAl_2O_4 and Al were also discussed by Shi et al [30] in detail. Using Equation (2)
 299 and corresponding thermodynamic data from the literature [30], we calculated the
 300 change in the Gibbs free energy for the reaction at the temperature of 750°C and 660
 301 °C is estimated as -44.4 kJ/mol and -7.4 kJ/mol, respectively. It means that the
 302 reaction time between the molten Al and MgO substrate is about 9 mins.

303

304 According to the DSC curves shown in Fig. 2, the peak for the chemical reaction is
 305 not observed, which means the influence of chemical reaction heat on the
 306 undercooling should be ignored. As mentioned, the thickness of the MgAl_2O_4 is on
 307 the nanometer scale, indicating that the reaction was not significant under our
 308 experimental conditions with a lower temperature and a shorter period of time for this
 309 reaction in comparison with previous research performed at 1023°C [24]. Another
 310 phenomenon found in this study is that the thickness of the produced MgAl_2O_4 is
 311 between 20-40nm as shown in Fig.3, which is far less than the thickness of the
 312 produced intermediated layer in Al/MgO shown in the previous research [8]. It may
 313 be due to the higher temperature and longer time that were employed to sufficiently
 314 provoke the interfacial reaction in the previous studies. ~~Therefore, it is reasonable to~~
 315 ~~conclude that the temperature and reaction time can significantly influence the~~
 316 ~~formation of a newly produced layer.~~

317 4.2 Orientation relationship induced by heterogeneous crystal

318 In our studies, the HRTEM images of MgO/MgAl₂O₄/Al regions show that there is a
 319 specific orientation relationship among the MgO substrate, reaction product MgAl₂O₄
 320 and Al. Orientation relationships were found to be of the kind shown in Fig. 7, namely
 321 $(100)_{\text{MgO}}// (100)_{\text{MgAl}_2\text{O}_4} // (100)_{\text{Al}}$, $[001]_{\text{MgO}} // [001]_{\text{MgAl}_2\text{O}_4} // [001]_{\text{Al}}$;
 322 $(110)_{\text{MgO}} // (110)_{\text{MgAl}_2\text{O}_4} // (110)_{\text{Al}}$, $[001]_{\text{MgO}} // [001]_{\text{MgAl}_2\text{O}_4} // [001]_{\text{Al}}$;
 323 $(111)_{\text{MgO}} // (111)_{\text{MgAl}_2\text{O}_4} // (111)_{\text{Al}}$, $[01\bar{1}]_{\text{MgO}} // [01\bar{1}]_{\text{MgAl}_2\text{O}_4}$.
 324



325
 326 Fig.7 Schematic illustration of interface matching for Al on (a) (100), (b) (110) and (c)
 327 (111) planes of MgO substrate.
 328

329 The interfacial free energy at the nucleating interface is the dominating factor in
 330 heterogeneous nucleation from a thermodynamic point of view. However, it is
 331 determined by chemical reaction, interface structure, wettability etc. Therefore, a
 332 simple description of this energy is difficult [23, 31, 32]. In practice, nucleating
 333 potency can be assessed by comparisons of the perfectness of the lattice matching. A
 334 smaller lattice misfit means a low lattice strain energy between two phases, and
 335 therefore a smaller undercooling required for nucleation [33]. A favored orientation
 336 relationship always corresponds to a low interfacial energy and a relatively stable
 337 mode thermodynamically [34].
 338

339 A theoretical approach to assess the nucleating potency is to calculate the lattice misfit
 340 at the interface between the substrate and matrix. According to Bramfitt's
 341 two-dimensional misfit theory [31] and the detected plane of a new crystal with the
 342 substrate (see Fig. 7), we figured out that the lattice misfit for Al(200)/MgAl₂O₄(400),
 343 Al(220)/MgAl₂O₄(220) and Al(111)/MgAl₂O₄(111) are all 1.17% in Al/MgO system.
 344 Here, the lattice misfit was calculated based on the coefficients of thermal expansion
 345 at the equilibrium melting point of pure Al of 660°C [35, 36]. It should be noted that
 346 the planes in this work are exactly the low index planes as stated in Bramfitt's model,
 347 which is consistent with the obtained misfit values from HRTEM.
 348

349 Moreover, the edge-to-edge model [12, 13, 37-40] was used to verify the orientation
 350 relationship between two components based on the actual crystal structures and the
 351 corresponding atom positions. The model is based on the matching of rows of atoms
 352 and habit plane across the interface. Al, MgO and MgAl₂O₄ have the same FCC
 353 structure with a lattice parameter of 0.4046nm, 0.4200nm and 0.8080nm, respectively.

354 Table 1 shows the space group, SG number and other parameters. As discussed in the
 355 literature [34], they have the same close packed directions and planes, and accordingly,
 356 the derived packed directions are [100], [110] and [111], while the planes are (100),
 357 (110) and (111) respectively.

358 As reported in the literature [12], the interatomic spacing misfit along the matching
 359 directions and the interplanar spacing misfit of matching planes were required to be
 360 less than 10% and 6%, respectively. Due to the interface reaction, the MgAl_2O_4 would
 361 take up the original interface of Al and MgO. Hence, the probable orientation
 362 relationship between Al and MgAl_2O_4 was calculated, with the result shown in Table
 363 2. It can be seen that there are three possible matching pairs, which are [100]
 364 Al//[100] MgAl_2O_4 , [110]Al//[110] MgAl_2O_4 , where the interatomic spacing misfits are
 365 all 0.16%. In the same way, the possible matching planes are (200) Al//(200)
 366 MgAl_2O_4 , (220) Al//(220) MgAl_2O_4 and (111) Al//(111) MgAl_2O_4 , which were
 367 calculated to be 0.16%. According to the edge-to-edge matching model, the matching
 368 directions should belong to the matching planes. Hence, the orientation relationship
 369 between Al and the MgO substrate could be predicted: (200)Al//(200) MgAl_2O_4 ,
 370 [001]Al//[001] MgAl_2O_4 or [011]Al//[011] MgAl_2O_4 ; (220)Al//(220) MgAl_2O_4 ,
 371 [001]Al//[001] MgAl_2O_4 or $[1\bar{1}0]$ Al// $[1\bar{1}0]$ MgAl_2O_4 ; (111)Al//(111) MgAl_2O_4 ,
 372 $[1\bar{1}0]$ Al// $[1\bar{1}0]$ MgAl_2O_4 , which can be confirmed by our experiment results.

373 Table 1. The space group, SG number, crystal system, lattice parameter and atom
 374 position of Al and MgO

Compound	Space group	SG number	Crystal system	Lattice parameter	Atom position
Al	Fm-3m	225	Cubic	0.4046	0.5,0.5,0
MgO	Fm-3m	225	Cubic	0.4200	Mg:0,0,0 O:0.5,0.5,0.5
MgAl_2O_4	Fd-3m	227	Cubic	0.8080	Mg:0.5,0.5,0.5 Al:0.125,0.125,0.125 O:0.264,0.264,0.264

375 Table 2. Interatomic and Interplanar spacing misfit of possible matching directions
 376 and planes between Al and MgO

Al/ MgAl_2O_4	f_1			Al/ MgAl_2O_4	f_2		
	[100]	[110]	[111]		(200)	(220)	(111)
[100]	0.16	29.40	13.54	(200)	0.16	29.4	15.28
[110]	29.40	0.16	22.28	(220)	5.87	0.16	8.69
[111]	18.48	15.28	29.40	(111)	13.54	22.28	0.16

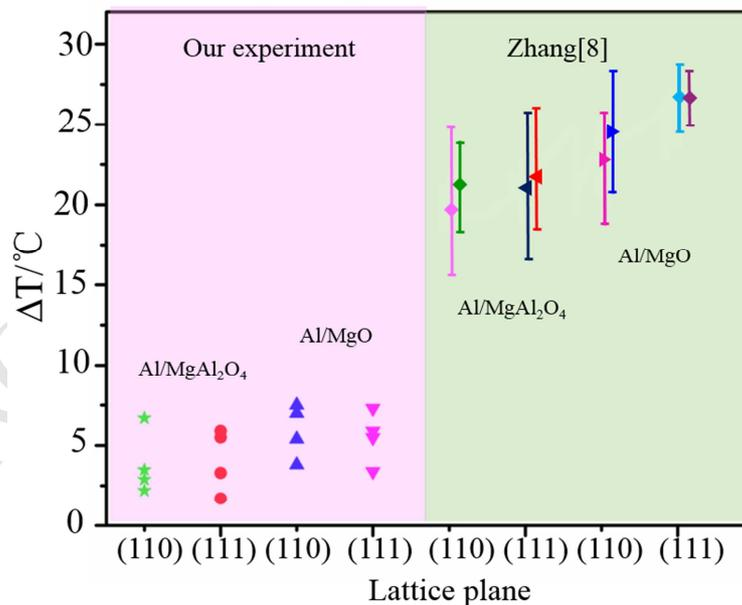
377 Note: f_1 is the interatomic spacing misfit of the close packed directions; f_2 is the
 378 interplanar spacing misfit of close packed planes

379
 380

381 4.3 Undercooling of molten Al nucleated on MgO substrate

382 Undercooling of 22-28°C and multi nucleation interfaces in Al/MgO were reported in
 383 the literature [8]. However, the undercooling of Al solidified on MgO substrate
 384 achieved in the present study is only between 3 to 8°C. It is mostly likely due to the
 385 significantly different measurement methods and experimental conditions between the
 386 current study and that employed in the literature [8, 11, 16]. Our experimental results
 387 have shown that the intermediate layer is only composed of MgAl₂O₄ phase, which is
 388 the new substrate for the nucleation of Al melt. In addition, the crystal orientation of
 389 newly produced MgAl₂O₄ phase is driven by the orientation of the original MgO
 390 substrate, and the perfect orientation matching between the produced MgAl₂O₄ and
 391 the original MgO are observed. Hence, in order to further confirm the undercooling of
 392 Al/MgO achieved in our study, DSC experiments of molten Al solidified on MgAl₂O₄
 393 (110) and (111) were performed and the corresponding undercooling is shown in Fig.8.
 394 It can be noted that the undercooling of the Al/MgAl₂O₄ system is very close to that of
 395 Al/MgO. This further confirms that the newly formed MgAl₂O₄ acted as the
 396 nucleation surface, and the initially terminated planes of the MgO substrates were
 397 isolated by the MgAl₂O₄.

398 The variation of undercooling for each Al/MgO(100), (110), (111) may be due to the
 399 essential feature of heterogeneous nucleation. According to the classical nucleation
 400 theory, there is a critical radius for the occurrence of nucleation. In practice, the
 401 structure or energy fluctuation is necessary to support the embryos whose size is
 402 closed to the critical size to trigger nucleation. It should be noted here that the size of
 403 embryos close to the critical size is not a point but a size range, which will lead to the
 404 nucleation temperature varied in a corresponding range as well as the variation of
 405 undercooling.



406

407 Fig.8 Undercooling of Al on MgAl₂O₄, and MgO substrates with different lattice
 408 planes. In contrast, the experimental undercooling includes the other data for liquid Al
 409 nucleated on the same substrates from literature [8].

410 In this study, a new and single substrate MgAl_2O_4 was formed through chemical
411 reaction. The new MgAl_2O_4 buffer layer has the same crystal structure with the
412 original MgO substrate other than the lattice parameter being twice that of the original
413 one. Comparing the experimentally determined orientation relationships with the
414 theoretically predicted orientation relationships, it is clear that the predictions from
415 the edge-to-edge matching model are consistent with the experimental results.
416 Theoretically, a good matching interface is more effective in triggering the nucleation
417 of a new crystal. The detected nucleation undercooling of Al/MgO in this study is also
418 confirmed by the results from $\text{Al}/\text{MgAl}_2\text{O}_4$.

419 5. Conclusion

420

421 In this study, thermal analysis and high resolution transmission electron microscopy
422 were used to study the nucleation behavior of high purity liquid Al on single crystal
423 MgO substrates by measuring the undercooling and the crystal orientation relationship
424 between nuclei and substrate. The results show that, due to the chemical reaction
425 between liquid Al and substrates, the original substrate MgO would be completely
426 replaced by reaction product MgAl_2O_4 . Consequently, the detected undercooling is
427 controlled by the newly produced MgAl_2O_4 . The interface characterization of
428 different exposed planes was observed by HRTEM, which is supported by a
429 well-defined orientation relationship with the equivalent lattice misfit of 1.17%, and
430 the orientation relationships of $(100)_{\text{MgO}} // (100)_{\text{MgAl}_2\text{O}_4} // (100)_{\text{Al}}$; $(110)_{\text{MgO}} //$
431 $(110)_{\text{MgAl}_2\text{O}_4} // (110)_{\text{Al}}$ and $(111)_{\text{MgO}} // (111)_{\text{MgAl}_2\text{O}_4} // (111)_{\text{Al}}$.

432 Acknowledgement

433 The authors thank J. Peng for stimulating discussions and TEM examination, X.
434 Liang for FIB analysis, the Instrumental Analysis & Research Center of SHU. This
435 work was supported by the National Natural Science Foundation of China (grant
436 number 51320105003, 51704192 and U1760204).

437 References

- 438 [1] D.F. W. Kurz, Fundamentals of Solidification, Trans Tech Publications, Switzerland, (1998).
439 [2] K.F. Kelton, A.L. Greer, D.M. Herlach, D. Holland-Moritz, The Influence of Order on the Nucleation
440 Barrier, MRS Bulletin, 29 (2011) 940-944.
441 [3] I. Maxwell, A. Hellawell, A simple model for grain refinement during solidification, Acta
442 Metallurgica, 23 (1975) 229-237.
443 [4] A.L. Greer, A.M. Bunn, A. Tronche, P.V. Evans, D.J. Bristow, Modelling of inoculation of metallic
444 melts: application to grain refinement of aluminium by Al-Ti-B , Acta Materialia, 48 (2000) 2823-2835.
445 [5] Q. Zeng, S. Xu, Thermodynamics and Characteristics of Heterogeneous Nucleation on Fractal
446 Surfaces, The Journal of Physical Chemistry C, 119 (2015) 27426-27433.
447 [6] M. Qian, J. Ma, The characteristics of heterogeneous nucleation on concave surfaces and
448 implications for directed nucleation or surface activity by surface nanopatterning, Journal of Crystal
449 Growth, 355 (2012) 73-77.
450 [7] F. Liu, D.Y. Xie, T. Majidi, G.-z. Zhu, Twin-assisted growth of nominally stable substrates underneath

- 451 dewetted Au nanoparticles, *Materials Characterization*, 113 (2016) 67-70.
- 452 [8] D. Zhang, L. Wang, M. Xia, N. Hari Babu, J.G. Li, Misfit paradox on nucleation potency of MgO and
453 MgAl₂O₄ for Al, *Materials Characterization*, 119 (2016) 92-98.
- 454 [9] M.E. Glicksman, W.J. Childs, Nucleation catalysis in supercooled liquid tin, *Acta Metallurgica*, 10
455 (1962) 925-933.
- 456 [10] S.H. Oh, Y. Kauffmann, C. Scheu, W.D. Kaplan, M. Rühle, Ordered Liquid Aluminum at the Interface
457 with Sapphire, *Science*, 310 (2005) 661.
- 458 [11] L. Wang, W. Lu, Q. Hu, M. Xia, Y. Wang, J.-g. Li, Interfacial tuning for the nucleation of liquid AlCu
459 alloy, *Acta Materialia*, 139 (2017) 75-85.
- 460 [12] M.X. Zhang, P.M. Kelly, Edge-to-edge matching and its applications: Part I. Application to the
461 simple HCP/BCC system, *Acta Materialia*, 53 (2005) 1073-1084.
- 462 [13] M.X. Zhang, P.M. Kelly, Edge-to-edge matching and its applications: Part II. Application to Mg–Al,
463 Mg–Y and Mg–Mn alloys, *Acta Materialia*, 53 (2005) 1085-1096.
- 464 [14] Z. Fan, An Epitaxial Model for Heterogeneous Nucleation on Potent Substrates, *Metallurgical and
465 Materials Transactions A*, 44 (2013) 1409-1418.
- 466 [15] T.E. Quested, A.L. Greer, Athermal heterogeneous nucleation of solidification, *Acta Materialia*, 53
467 (2005) 2683-2692.
- 468 [16] J. Li, L. Wang, X. Zhong, M. Xia, S.J. Haigh, P. Schumacher, Cu segregation on the interface
469 between Al₂O₃ substrate and Al-1.4Cu alloy, *Materials Characterization*, 129 (2017) 300-304.
- 470 [17] L. Wang, L. Yang, D. Zhang, M. Xia, Y. Wang, J.G. Li, The Role of Lattice Misfit on Heterogeneous
471 Nucleation of Pure Aluminum, *Metallurgical and Materials Transactions A*, 47 (2016) 5012-5022.
- 472 [18] G. Wilde, J.L. Sebright, J.H. Perepezko, Bulk liquid undercooling and nucleation in gold, *Acta
473 Materialia*, 54 (2006) 4759-4769.
- 474 [19] G. Wilde, C. Santhaweesuk, J.L. Sebright, J. Bokeloh, J.H. Perepezko, Kinetics of heterogeneous
475 nucleation on intrinsic nucleants in pure fcc transition metals, *Journal of Physics: Condensed Matter*,
476 21 (2009) 464113.
- 477 [20] M.P. De Cicco, L.-S. Turng, X. Li, J.H. Perepezko, Nucleation Catalysis in Aluminum Alloy A356 Using
478 Nanoscale Inoculants, *Metallurgical and Materials Transactions A*, 42 (2011) 2323-2330.
- 479 [21] G.I. Tóth, G. Tegze, T. Pusztai, L. Gránásy, Heterogeneous Crystal Nucleation: The Effect of Lattice
480 Mismatch, *Physical Review Letters*, 108 (2012) 025502.
- 481 [22] A.J. Brown, H.B. Dong, P.B. Howes, C.L. Nicklin, In situ observation of the orientation relationship
482 at the interface plane between substrate and nucleus using X-ray scattering techniques, *Scripta
483 Materialia*, 77 (2014) 60-63.
- 484 [23] H.T. Li, Y. Wang, Z. Fan, Mechanisms of enhanced heterogeneous nucleation during solidification
485 in binary Al–Mg alloys, *Acta Materialia*, 60 (2012) 1528-1537.
- 486 [24] K. Kim, Detection of a Layer of Al₂O₃ at the Interface of Al/MgAl₂O₄ by High-Resolution
487 Observation Using Dual-Beam FIB and TEM, *Metallography, Microstructure, and Analysis*, 3 (2014)
488 233-237.
- 489 [25] H. Fujii, H. Nakae, Equilibrium contact angle in the magnesium oxide/aluminium system, *Acta
490 Materialia*, 44 (1996) 3567-3573.
- 491 [26] A.J. McEvoy, R.H. Williams, I.G. Higginbotham, Metal/non-metal interfaces. The wetting of
492 magnesium oxide by aluminium and other metals, *Journal of Materials Science*, 11 (1976) 297-302.
- 493 [27] J. Morgiel, N. Sobczak, M. Pomorska, R. Nowak, First stage of reaction of molten Al with MgO
494 substrate, *Materials Characterization*, 103 (2015) 133-139.

- 495 [28] R. Nowak, N. Sobczak, E. Sienicki, J. Morgiel, Structural Characterization of Reaction Product
496 Region in Al/MgO and Al/MgAl₂O₄ Systems, *Solid State Phenomena*, 172-174 (2011) 1273-1278.
- 497 [29] P. Shen, H. Fujii, T. Matsumoto, K. Nogi, Wetting and reaction of MgO single crystals by molten Al
498 at 1073–1473 K, *Acta Materialia*, 52 (2004) 887-898.
- 499 [30] L. Shi, P. Shen, D. Zhang, Q. Jiang, Reactive wetting of amorphous silica by molten Al–Mg alloys
500 and their interfacial structures, *Applied Surface Science*, 377 (2016) 340-348.
- 501 [31] B.L. Bramfitt, The effect of carbide and nitride additions on the heterogeneous nucleation
502 behavior of liquid iron, *Metallurgical Transactions*, 1 (1970) 1987-1995.
- 503 [32] X. Cao, J. Campbell, The nucleation of Fe-Rich phases on oxide films in Al-11.5Si-0.4Mg cast alloys,
504 *Metallurgical and Materials Transactions A*, 34 (2003) 1409-1420.
- 505 [33] V.B. Turnbull D, Nucleation Catalysis, *Industrial & Engineering Chemistry*, 44 (1952) 7.
- 506 [34] Y. Liu, Y. Huang, Z. Xiao, Study of orientation relationship between Al matrix and several typical
507 inclusions in Al alloy by edge-to-edge matching model, *Journal of Materials Research*, 32 (2017)
508 2092-2099.
- 509 [35] J.L. Smialek, M.A. Gedwill, P.K. Brindley, Cyclic oxidation of aluminide coatings on Ti₃Al+Nb,
510 *Scripta Metallurgica et Materialia*, 24 (1990) 1291-1296.
- 511 [36] B.H. Avedesian M M, ASM speciality handbook: magnesium and magnesium alloys, ASM
512 international, 18 (1999) 2.
- 513 [37] P.M. Kelly, M.X. Zhang, Comments on edge-to-edge matching and the equivalence of the invariant
514 line, Δg and Moiré Fringe approaches to the crystallographic features of precipitates, *Scripta*
515 *Materialia*, 52 (2005) 679-682.
- 516 [38] M.X. Zhang, P.M. Kelly, Edge-to-edge matching model for predicting orientation relationships and
517 habit planes—the improvements, *Scripta Materialia*, 52 (2005) 963-968.
- 518 [39] P.M. Kelly, M.X. Zhang, Edge-to-edge matching—The fundamentals, *Metallurgical and Materials*
519 *Transactions A*, 37 (2006) 833-839.
- 520 [40] H.M. Fu, D. Qiu, M.X. Zhang, H. Wang, P.M. Kelly, J.A. Taylor, The development of a new grain
521 refiner for magnesium alloys using the edge-to-edge model, *Journal of Alloys and Compounds*, 456
522 (2008) 390-394.

- (1) Only MgAl_2O_4 layer is produced at the interface of Al/MgO system due to chemical reaction occurred from 750°C to 660 °C.
- (2) The well-defined orientation relationship is achieved at the interface of Al/ MgAl_2O_4 /MgO.
- (3) MgAl_2O_4 layer has a significant influence on the heterogeneous nucleation of Al.